Robust Stabilizing Control for Oscillatory Base Manipulators by Implicit Lyapunov Method

Yufei Guo (guoyufei_1985@163.com)
Wuhan University of Science and Technology https://orcid.org/0000-0002-5346-3434
Baolin Hou
Nanjing University of Science and Technology
Shengyue Xu
Wuhan University of Science and Technology
Ruilin Mei
Wuhan University of Science and Technology
Zhigang Wang
Wuhan University of Science and Technology
Van Thanh Huynh
Deakin University

Research Article

Keywords: Autoloaders, Oscillatory base manipulators, Implicit Lyapunov function, Robust Control, Self-tuning PD control

Posted Date: May 28th, 2021

DOI: https://doi.org/10.21203/rs.3.rs-528002/v1

Version of Record: A version of this preprint was published at Nonlinear Dynamics on March 11th, 2022.
See the published version at https://doi.org/10.1007/s11071-022-07321-w.

Nonlinear Dynamics manuscript No.
(will be inserted by the editor)

Robust stabilizing control for oscillatory base manipulators by implicit Lyapunov method

Yufei Guo · Baolin Hou · Shengyue Xu · Ruilin Mei · Zhigang Wang · Van Thanh Huynh

Received: date / Accepted: date

Abstract Oscillatory base manipulators (OBMs) are a kind of mechanical systems suffering from unexpected base oscillations. The oscillations affect tremendously system stability. Various control methods have been explored, but most of them require measurement or prediction of the oscillations. This study is concerned with a novel OBM–the autoloader, which are used in modern, autonomous main battle tanks. The base oscillation of the autoloader is hard to be obtained in practice. Furthermore, control synthesis for autoloaders is complicated with intrinsic payload uncertainty and actuator saturation. To address these issues, a novel robust control scheme is proposed in this work relying on the implicit Lyapunov method. Moreover, a novel two-Degree-of-Freedom manipulator operating on a vibrating base is constructed to realize the proposed control. To the best of the authors' knowledge, this is the first study considering both control and hardware implementation for the OBM-like autoloaders. Experimental results demonstrate that, although without prior information of the base oscillation, the proposed controller exhibits good robustness against the base oscillation and payload uncertainty.

Keywords Autoloaders · Oscillatory base manipulators · Implicit Lyapunov function · Robust Control · Self-tuning PD control

Yufei Guo(✉) · Shengyue Xu · Ruilin Mei · Zhigang Wang
Key Laboratory of Metallurgical Equipment and Control Technology of Ministry of Education,
School of Machinery and Automation,
Wuhan University of Science and Technology,
Wuhan 430081, China
E-mail: guoyufei_1985@163.com

Yufei Guo
Institute of Robotics and Intelligent Systems,
Wuhan University of Science and Technology,
Wuhan 430081, China

Baolin Hou
Shool of Mechanical Engineering,
Nanjing University of Science and Technology,
Nanjing, 210094, China

Van Thanh Huynh
Shool of Engineering,
Deakin University,
Geelong, VIC 3217, Australia

1 Introduction

Main Battle Tanks (MBTs) are tracked vehicles working on harsh and random terrains, and equipped with actuators and manipulators internally to facilitate the vehicle operation. Considerable efforts have been devoted to improving automation of the MBTs, one of which is adoption of the autoloader manipulators. The autoloader is used to automate the process of loading objects, e.g. ammunition objects, inside the vehicle [1]. Compared with the manual loader with human involvement in the operation, the autoloader has merits of small volume, light weight and fast motion.

However, most of the existing autoloaders are facing the problem of poor control accuracy due to its harsh working conditions [2]. Specifically, when the tracked vehicle is moving and the autoloader is simultaneously operating at speed inside the vehicle, the chassis (the mounted base of the autoloader) will suffer from extreme oscillations caused by external uneven terrains and internal interaction between the autoloader and the vehicle, as shown in Fig. 1. The base oscillation brings challenges to operation of both the manual loader and autoloader. Currently, the manual loading process is mostly operated while the vehicle is stationary. For the existing autoloaders, most of them used traditional control methods (such as the proportional derivative control), which offered less robustness against the base oscillation and in

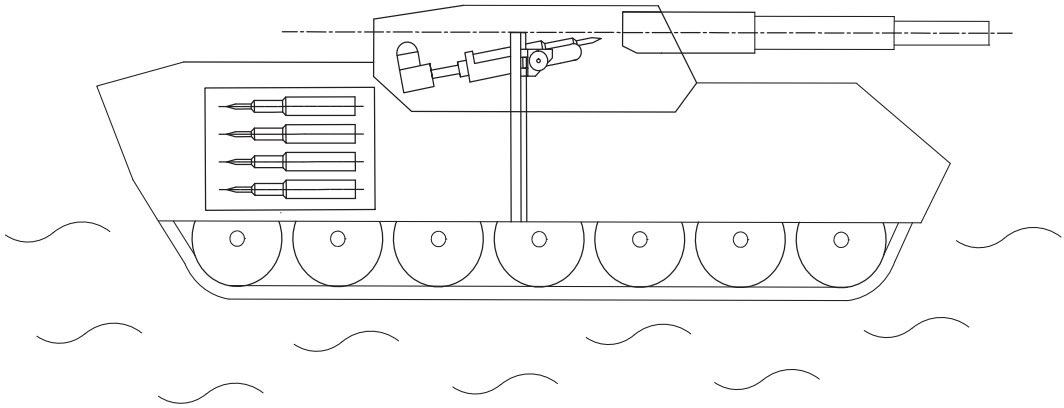

Fig. 1 MBTs autoloader with oscillatory chassis

turn brought in poor positioning accuracy. An additional mechanical brake device was usually used to guarantee the control performance, but this led to unexpected contact forces and in turn the poor reliability of the entire system.

In practice, numerous mechanical systems are also facing the base-oscillation-induced problem, such as macro-micro manipulators, space manipulators, UVMs (underwater vehicle manipulators), offshore cranes, and so forth. They can all be categorized as oscillatory-base manipulators (OBMs) [3, 4]. For the macro-micro manipulator, which is composed of a rigid link and a flexible link, the base oscillation is mainly from the structural vibration of the flexible link [5, 6]. For the space manipulator, due to working in the weightless environment [7, 8], even minimal impact between the target and the manipulator can cause huge undesired oscillation of the base (space craft). For UVMs, the mounted base (underwater vehicles) is usually subject to a class of fluid disturbance caused by oceanic current [9-12]. Offshore cranes, also known as ship-mounted cranes, are also suffering from the oceanic-wave-induced oscillation [13-15].

In general, OBMs can be classified in three ways from different perspectives, as shown in Tab. 1. First, it can be classified based on whether oscillations are derived from external disturbances or internal interactions. Obviously, autoloaders together with offshore cranes and UVMs belong to the first type, while space manipulators and macro/micro manipulators are the second type. Moreover, OBMs can be classified based on whether information about the base oscillation can be obtained in advance or not. Except for autoloaders, the base oscillation of most OBMs can be measured or predicted in practice. In addition, OBMs can be classified according to their working task space, i.e. either in inertia or non-inertial frame. The MBTs autoloader belong to the latter type, but most of other OBMs are the former type. In this paper, for the sake of simplicity, we give code names for each type of OBMs. For instance, OBMs with base oscillations from external disturbances are named as type A1, where the character indicates the classification method and the number indicates a type under the classification.

The control objective of different OBMs is similar, which can be stated as: 'Achieving robust stabilizing or tracking control of manipulators suffering from base-oscillation-caused perturbations'. For type A1 OBMs, the primary issue is the base oscillation suppression. Various control techniques have been developed, such as adaptive suppression approach [24], feed-forward compensation approach [4, 7, 25-27], active reaction null-space control [18, 19], vision-based predictive method [28-30], and so forth. However, for type A2 OBMs, due to the base oscillation comes from external excitations, it is impossible to be suppressed or eliminated directly. Fortunately, for some of them (type B1), the prior information

Tab. 1 Summary of OBMs classifications

Classification method	Type	Macro/micro manipulators	Space manipulators	UVMs	Offshore cranes	Autoloaders of MBTs
A-origination of oscillations	1-internal interactions	√	√			
	2-external disturbances			√	√	√
B-oscillations available	1-yes	√	√	√	√	
	2-not					√
C-working task space	1-inertial frame	√	√	√	√	
	2-noninertial frame					√

of the base oscillation can be used to simplify the control design [31-33]. For example, Toda has proposed several control methods for ship-mounted manipulators based on that the base oscillation's frequency range can be obtained by some prediction method [3, 34, 35].

Although there are a lot of studies on the control of OBMs, several problems are still unaddressed for MBTs autoloaders (type A2-B2-C2 OBMs). Specially, the base oscillation, which is mainly caused by both uneven terrains and internal interaction between the autoloaders and vehicle chassis, cannot be suppressed by current active or passive damping control. Moreover, its prior information is difficult to predict or measure in practice. Thirdly, for MBTs autoloaders, because of operation in non-inertial frames (based-fixed coordinates), greater nonlinearities such as Coriolis and centrifugal forces are induced. This brings much more challenging factors to the control synthesis. In addition, for the control design for the autoloaders, the payload uncertainty and actuator saturation also bring in great challenges, but most of current studies did not consider these issues in depth.

This paper addresses the above problems and make the following contributions:

(1) We firstly propose a general dynamical model of the autoloader suffering from base oscillations. Due to the reality that the base has a much greater inertia than the autoloader, the base oscillation's effect is regarded as the uncertain perturbation of the autoloader, but the autoloader's reaction on the base is ignored. Then, the dynamical decoupling between the autoloader and the base is easily achieved by the second Lagrange Equation. Moreover, the base oscillation is firstly divided into three parts in this paper, which greatly simplified the model building of the system.

(2) A novel roust control based on implicit Lyapunov function [36,37] is developed stabilize the autoloader. It can be considered a parameter-varying PD control whose control gains are automatically tuned to guarantee stability of the system. The proposed control has good robustness against the base-oscillation-caused uncertainty as there is no need for the base oscillation's prior information. Moreover, the control input is always norm-bounded.

(3) The hardware experiments for the robust stabilizing control of MBT autoloaders are proposed for the first time. The experiments certify the proposed control's asymptotic stability against not only base oscillations but also payload uncertainty.

The organization of the paper is as follows. In Section 2, the autoloader system's configuration as well as the uncertain dynamics model is presented with some analysis. Section 3 presents the process of the control design and stability analysis of which. The Section 4 provides the experimental implementation and results, and the section 5 gives the paper's conclusions finally.

2 Preliminaries

2.1 System configuration

A novel 2-DOF (degree of freedom) autoloader was designed in our previous research, as presented in Fig. 2.

As shown, the autoloader mainly consists of three parts: a transfer device, a lifting device and a mounted frame. The automatically loading process of the autoloader includes the following four step motions. Firstly, the transfer device grasps an object, e.g. the ammunition object. Then, the lifting device hoists the object to a pre-specified position. Thirdly, the transfer device flips the object to make it aligned with a succeeding device. Finally, the object is loaded into the succeeding device. From the perspective of positioning control, only the motions of the second and third steps need to be took into account. Moreover, the base oscillation also needs to be considered in the control design. Therefore, the autoloader with the base can be simplified as a 3-links apparatus. In addition, the base mainly suffers from three directions of oscillations in practice, as as show in the figure.

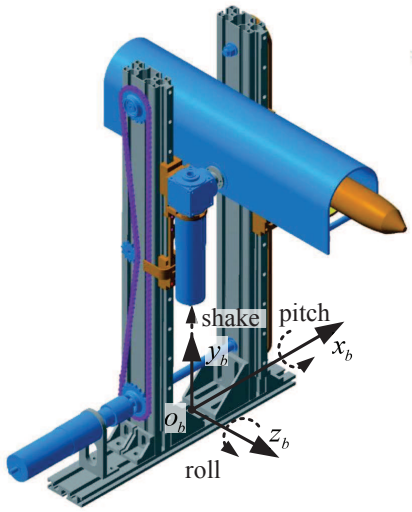

Fig. 2 Virtual prototype of the autoloader

2.2 Dynamic Model

Based on above analysis, a simplified model for the autoloader with the oscillatory base is established, as shown in Fig. 3, where *xoy* and *XOY* denote the inertial and non-inertial coordinate, respectively; the *Y* axis is along the gravitational direction; B_1, B_2 and B_3 represent the oscillatory base, the lifting device and the revolving device (including the payload), respectively; C_2 and C_3 are the centroid of B_2 and B_3, respectively; y_{r2} and θ_3 denote the linear displacement of the lifting device and the angular position of the

revolving device, respectively; y_1, θ_{z1} and θ_{x1} denote the movements of the base along three different directions; L_1 and L_3 represent geometric parameters as shown in the figure.

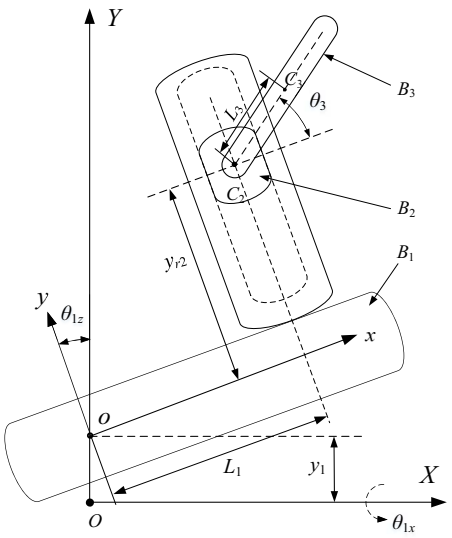

Fig. 3 Simplified model of the autoloader with oscillatory base

The dynamics of the above simplified model can be derived using the second Lagrange equation. Firstly, for simplicity, the base oscillation is divided into three parts: the pitch, shake and roll oscillations, respectively. Furthermore, as mentioned before, the tank chassis has a much greater inertia than the autoloader, so the base oscillation's effect is regarded as the uncertain perturbation of the autoloader, but the autoloader's reaction on the base is ignored. Finally, regarding $\boldsymbol{q} = [y_{r2}, \theta_3]^T$ as the system's state variables, the uncertain dynamical model of the autoloader with base oscillation is established as follows:

$$\boldsymbol{H}(\boldsymbol{q})\ddot{\boldsymbol{q}} + \boldsymbol{C}(\boldsymbol{q},\dot{\boldsymbol{q}})\dot{\boldsymbol{q}} + \boldsymbol{G}(\boldsymbol{q}) = \boldsymbol{S} + \boldsymbol{U}, \tag{1}$$

where $\boldsymbol{H}(\boldsymbol{q})$ denotes the inertia matrix, the Coriolis/centripetal force term is $\boldsymbol{C}(\boldsymbol{q},\dot{\boldsymbol{q}})\dot{\boldsymbol{q}}$, the gravity force is presented using $\boldsymbol{G}(\boldsymbol{q})$, the control needed to be constructed is $\boldsymbol{U}$, and $\boldsymbol{S}$ denotes the uncertain perturbation from base oscillations (payload uncertainty could also be included into this term). Moreover, each term of Eq. (1) is as follows:

$$\boldsymbol{H}(\boldsymbol{q}) = \begin{bmatrix} m_2+m_3 & m_3L_3\cos\theta_3 \\ m_3L_3\cos\theta_3 & m_3L_3^2+J_3 \end{bmatrix},$$

$$\boldsymbol{C}(\boldsymbol{q},\dot{\boldsymbol{q}})\dot{\boldsymbol{q}} = \begin{bmatrix} -m_3L_3\sin(\theta_3)\dot{\theta}_3^2 \\ 0 \end{bmatrix},$$

$$\boldsymbol{G}(\boldsymbol{q}) = \begin{bmatrix} (m_2+m_3)g \\ m_3gL_3\cos\theta_3 \end{bmatrix},$$

where J_3 is the the revolving device's inertia moment, m_3 is the revolving device's mass, m_2 is the lifting part's mass, and g is the gravitational acceleration.

Moreover, $\boldsymbol{S} = [S_{1s}, S_{2s}]^T$, $[S_{1p}, S_{2p}]^T$ and $[S_{1r}, S_{2r}]^T$ denote uncertain perturbation caused by the shake, pitch and roll oscillations, respectively. Particularly, we can obtain

$$\begin{aligned}
S_{1s} &= -(m_2+m_3)\ddot{y}_1, \\
S_{2s} &= -m_3L_3\cos\theta_3\ddot{y}_1, \\
S_{1p} &= -((m_2L_1+m_3L_1+m_3L_3\cos\theta_3)\ddot{\theta}_{1z} \\
&\quad - 2m_3L_3\sin\theta_3\dot{\theta}_{1z}\dot{\theta}_3 - (m_2y_{r2}+m_3y_{r2}+m_3L_3\sin\theta_3)\dot{\theta}_{1z}^2) \\
&\quad - ((m_2+m_3)g\cos\theta_{1z} - (m_2+m_3)g), \\
S_{2p} &= -((J_3+m_3L_3^2+m_3L_1L_3\cos\theta_3+m_3L_3y_{r2}\sin\theta_3)\ddot{\theta}_{1z} \\
&\quad + 2m_3L_3\sin\theta_3\dot{\theta}_{1z}\dot{y}_{r2} + (m_3L_1L_3\sin\theta_3 \\
&\quad - m_3L_3y_{r2}\cos\theta_3)\dot{\theta}_{1z}^2) \\
&\quad - (m_3gL_3\cos(\theta_{1z}+\theta_3) - m_3gL_3\cos\theta_3), \\
S_{1r} &= (m_2+m_3)y_{r2}\dot{\theta}_{1x}^2 + m_3L_3\sin\theta_3\dot{\theta}_{1x}^2 - (m_2+m_3)g\cos\theta_2 \\
&\quad - (m_2+m_3)g, \\
S_{2r} &= m_3y_{r2}\dot{\theta}_{1x}^2 + m_3L_3\sin\theta_3\dot{\theta}_{1x}^2 - m_3gL_3\cos\theta_{1x}\cos\theta_3 \\
&\quad - m_3gL_3\cos\theta_3.
\end{aligned}$$

Generally, the dynamical model described by Eq. (1) possesses peculiar properties of robotic manipulators [38]. Below are the properties that will be used in the development of the main results of this paper.

Property 1: $\boldsymbol{H}(\boldsymbol{q})$ is a symmetrical matrix, and it is uniformly bounded from above and below, i.e.

$$m\boldsymbol{z}^2 \le \|\boldsymbol{z}^T\boldsymbol{H}(\boldsymbol{q})\boldsymbol{z}\| \le M\boldsymbol{z}^2, \tag{2}$$

where m and M are positive constants, $\boldsymbol{z}$ is an arbitrary vector. In this paper, $\|*\|$ denotes the vector or matrix's Euclidean norm.

Property 2: $\boldsymbol{H}(\boldsymbol{q})$ also satisfies the condition that its partial derivative is uniformly norm bounded, i.e.

$$\|\frac{\partial \boldsymbol{H}(\boldsymbol{q})}{\partial q_i}\| \le D, D > 0. \tag{3}$$

Property 3: The following matrix:

$$\boldsymbol{N}(\boldsymbol{q},\dot{\boldsymbol{q}}) = \dot{\boldsymbol{H}}(\boldsymbol{q}) - 2\boldsymbol{C}(\boldsymbol{q},\dot{\boldsymbol{q}}), \tag{4}$$

is an anti-symmetric matrix. Specially, for any vector $\boldsymbol{z}$, there is

$$\boldsymbol{z}^T\boldsymbol{N}(\boldsymbol{q},\dot{\boldsymbol{q}})\boldsymbol{z} = 0.$$

Property 4: In practice, $\boldsymbol{S}$ satisfies the following bounded conditions:

$$\|\boldsymbol{S}\| \le S_0, S_0 > 0. \tag{5}$$

Property 5: The control input should also be bounded in norm in practice. That means

$$\|\boldsymbol{U}\| \leq U_0, U_0 > 0. \tag{6}$$

Property 6: There exist a positive constant g_0 such that,

$$\|\frac{\partial P(\boldsymbol{q})}{\partial \boldsymbol{q}}\| = \|\boldsymbol{G}(\boldsymbol{q})\| \leq g_0, \tag{7}$$

where $P(\boldsymbol{q})$ denote gravitational energy of the system.

Now, let us give description to the considered problem.

Problem statement: Constructing a control $\boldsymbol{U}$ for system (1) affected by unpredictable perturbations $\boldsymbol{S}$ of Eq. (5) so that the closed-loop controlled system is robustly stabilized and simultaneously satisfies the given constraint shown in Eq. (6).

3 Control design

In this section, a robust control based on the implicit Lyapunov function is proposed to solve the above-stated problem. Moreover, stability analysis of the closed-loop, uncertain system is carried out. In addition, for the purpose of comparison, a traditional constant PD controller with gravity compensator is also presented.

3.1 Constant PD control

For system (1), if $\boldsymbol{S} = 0$, a simple PD control combined with gravity compensation can stabilize the system.

Specifically, introducing

$$\boldsymbol{U} = \boldsymbol{k}_p(\boldsymbol{q}_d - \boldsymbol{q}) - \boldsymbol{k}_d\dot{\boldsymbol{q}} + \boldsymbol{G}(\boldsymbol{q}), \tag{8}$$

where $\boldsymbol{q}_d$ is the setting reference point. For simplicity, we set $\boldsymbol{q}_d = 0$ here. Also, $\boldsymbol{k}_d$ and $\boldsymbol{k}_p$ represent the constant gains of the PD controller, both of which are positive definite matrices.

Furthermore, we choose a Lyapunov function as

$$V = \frac{1}{2}\dot{\boldsymbol{q}}^T\boldsymbol{H}(\boldsymbol{q})\dot{\boldsymbol{q}} + \frac{1}{2}\boldsymbol{q}^T\boldsymbol{k}_p\boldsymbol{q}. \tag{9}$$

Since $\boldsymbol{H}(\boldsymbol{q})$ and $\boldsymbol{k}_p$ are positive definite, we can conclude that the Lyapunov function V is also positive definite.

Then, differentiating the function along the system trajectory, we can obtain

$$\dot{V} = -\frac{1}{2}\dot{\boldsymbol{q}}^T\boldsymbol{k}_d\dot{\boldsymbol{q}} \leq 0. \tag{10}$$

Due to Eqs. (9) and (10), it can be concluded that system (1) with $\boldsymbol{S} = 0$ is asymptotically stable at $(\boldsymbol{q}, \dot{\boldsymbol{q}}) = (\boldsymbol{q}_d, 0)$.

3.2 Implicit Lyapunov control

However, when $\boldsymbol{S} \neq \boldsymbol{0}$, the system is with uncertainty and becomes

$$\boldsymbol{H}(\boldsymbol{q})\ddot{\boldsymbol{q}} + \boldsymbol{C}(\boldsymbol{q}, \dot{\boldsymbol{q}})\dot{\boldsymbol{q}} = \boldsymbol{S} - \boldsymbol{k}_p\boldsymbol{q} - \boldsymbol{k}_d\dot{\boldsymbol{q}}. \tag{11}$$

The aforementioned constant PD controller is no long valid in this case. It could not guarantee stability of the uncertain system. For simplicity, the gravity term $\boldsymbol{G}(\boldsymbol{q})$ is also considered as part of $\boldsymbol{S}$ here. This is because that the gravity compensation approach is very much accurate-model-dependent, which is hard to realize in practice. Additionally, for simplicity, $\boldsymbol{H}(\boldsymbol{q})$, $\boldsymbol{G}(\boldsymbol{q})$, etc., are abbreviated as $\boldsymbol{H}$, $\boldsymbol{G}$,etc. in the following part of this paper.

For system (1), we redefine $\boldsymbol{k}_d$ and $\boldsymbol{k}_p$ as,

$$\boldsymbol{k}_d = \alpha\boldsymbol{H}, \ \ \boldsymbol{k}_p = \beta\boldsymbol{I}, \tag{12}$$

$$\alpha = \sqrt{\frac{\beta}{M}}, \ \ \beta = \frac{3U_0^2}{8V}, \tag{13}$$

$$V = \frac{1}{2}\dot{\boldsymbol{q}}^T\boldsymbol{H}\dot{\boldsymbol{q}} + \frac{1}{2}\beta\boldsymbol{q}^2 + \frac{1}{2}\alpha\dot{\boldsymbol{q}}^T\boldsymbol{H}\boldsymbol{q}, \tag{14}$$

where V is a candidate Lyapunov function, $\boldsymbol{I}$ is an identity matrix.

Obviously, above Lyapunov function as well as control gains $\boldsymbol{k}_d$, $\boldsymbol{k}_p$ are implicit function of state variables.

Next, V will be proved to be a real Lyapunov function. Particularly, we will give V's positive definiteness, and negative definiteness of $\dot{V}$.

Stability analysis:

Firstly, we will estimate the bound of V .

In particular, it could been obtained the following inequality by Cauchy inequality, Eq. (13).

$$\begin{aligned}\|\alpha\dot{\boldsymbol{q}}^T\boldsymbol{H}\boldsymbol{q}\| &\leq \alpha\sqrt{(\dot{\boldsymbol{q}}^T\boldsymbol{H}\dot{\boldsymbol{q}})(\boldsymbol{q}^T\boldsymbol{H}\boldsymbol{q})} \\ &\leq \frac{1}{2}\dot{\boldsymbol{q}}^T\boldsymbol{H}\dot{\boldsymbol{q}} + \frac{1}{2}\alpha^2\boldsymbol{q}^T\boldsymbol{H}\boldsymbol{q} \leq \frac{1}{2}\dot{\boldsymbol{q}}^T\boldsymbol{H}\dot{\boldsymbol{q}} + \frac{1}{2}\beta\boldsymbol{q}^2.\end{aligned} \tag{15}$$

Combing Eq. (14) and inequality (15), we finally obtain the bound of V as follows,

$$\frac{1}{4}(\dot{\boldsymbol{q}}^T\boldsymbol{H}\dot{\boldsymbol{q}} + \beta\boldsymbol{q}^2) \leq V \leq \frac{3}{4}(\dot{\boldsymbol{q}}^T\boldsymbol{H}\dot{\boldsymbol{q}} + \beta\boldsymbol{q}^2)). \tag{16}$$

Obviously, V has the property of global positive definiteness, for any $(\boldsymbol{q}, \dot{\boldsymbol{q}}) \neq (0, 0)$,

Secondly, the derivative of the Lyapunov function will be evaluated.

Particularly, by differentiating both sides of the Eq. (14), it could be obtained

$$\begin{aligned}\dot{V} = &\frac{1}{2}\alpha\dot{\boldsymbol{q}}^T\dot{\boldsymbol{H}}\boldsymbol{q} + \frac{1}{2}\alpha\ddot{\boldsymbol{q}}^T\boldsymbol{H}\boldsymbol{q} + \frac{1}{2}\alpha\dot{\boldsymbol{q}}^T\boldsymbol{H}\dot{\boldsymbol{q}} \\ &+ \frac{1}{2}\dot{\alpha}\dot{\boldsymbol{q}}^T\boldsymbol{H}\boldsymbol{q} + \frac{1}{2}\dot{\boldsymbol{q}}^T\dot{\boldsymbol{H}}\dot{\boldsymbol{q}} + \dot{\boldsymbol{q}}^T\boldsymbol{H}\ddot{\boldsymbol{q}} + \beta\boldsymbol{q}^T\dot{\boldsymbol{q}} + \frac{1}{2}\dot{\beta}\boldsymbol{q}^2,\end{aligned} \tag{17}$$

with

$$\dot{\alpha} = -\frac{\alpha}{2V}\dot{V}, \quad \dot{\beta} = -\frac{\beta}{V}\dot{V}, \tag{18}$$

Moreover, by premultiplying $\boldsymbol{H}^{-1}$, we can rewrite Eq. (11) as

$$\ddot{\boldsymbol{q}} = \boldsymbol{H}^{-1}(-\boldsymbol{k}_p\boldsymbol{q} - \boldsymbol{k}_d\dot{\boldsymbol{q}} - \boldsymbol{C}\dot{\boldsymbol{q}} + \boldsymbol{S}), \tag{19}$$

Substituting Eqs. (12), (18) and (19) into Eq. (17), we obtain

$$\begin{aligned}
&\dot{V}(1 + \frac{1}{2}\frac{\beta}{V}\boldsymbol{q}^2 + \frac{1}{4}\frac{\alpha}{V}\dot{\boldsymbol{q}}^T\boldsymbol{H}\boldsymbol{q}) \\
&= -\alpha(\frac{1}{2}\dot{\boldsymbol{q}}^T\boldsymbol{H}\dot{\boldsymbol{q}} + \frac{1}{2}\alpha\boldsymbol{q}^T\boldsymbol{H}\dot{\boldsymbol{q}} + \frac{1}{2}\beta\boldsymbol{q}^T\boldsymbol{q}) \\
&\quad + \frac{1}{2}\dot{\boldsymbol{q}}^T\dot{\boldsymbol{H}}\dot{\boldsymbol{q}} - \dot{\boldsymbol{q}}^T\boldsymbol{C}\dot{\boldsymbol{q}} + \frac{1}{2}\alpha\dot{\boldsymbol{q}}^T\dot{\boldsymbol{H}}\boldsymbol{q} \\
&\quad - \frac{1}{2}\alpha\boldsymbol{q}^T\boldsymbol{C}\dot{\boldsymbol{q}} + \dot{\boldsymbol{q}}^T\boldsymbol{S} + \frac{1}{2}\alpha\boldsymbol{q}^T\boldsymbol{S}.
\end{aligned} \tag{20}$$

According to the anti-symmetry of matrix $\boldsymbol{N}$ (*Property 3*) , Eq. (20) could be rewritten as

$$\begin{aligned}
&\dot{V}(1 + \frac{1}{2}\frac{\beta}{V}\boldsymbol{q}^2 + \frac{1}{4}\frac{\alpha}{V}\dot{\boldsymbol{q}}^T\boldsymbol{H}\boldsymbol{q}) \\
&= -\alpha(\frac{1}{2}\dot{\boldsymbol{q}}^T\boldsymbol{H}\dot{\boldsymbol{q}} + \frac{1}{2}\alpha\boldsymbol{q}^T\boldsymbol{H}\dot{\boldsymbol{q}} + \frac{1}{2}\beta\boldsymbol{q}^T\boldsymbol{q}) \\
&\quad + \frac{1}{2}\alpha\dot{\boldsymbol{q}}^T\dot{\boldsymbol{H}}\boldsymbol{q} - \frac{1}{2}\alpha\boldsymbol{q}^T\boldsymbol{C}\dot{\boldsymbol{q}} + \dot{\boldsymbol{q}}^T\boldsymbol{S} + \frac{1}{2}\alpha\boldsymbol{q}^T\boldsymbol{S}.
\end{aligned} \tag{21}$$

Moreover, due to the vector of the Coriolis/centripetal forces $\boldsymbol{C}\dot{\boldsymbol{q}}$ satisfies the following condition [38].

$$\boldsymbol{C}\dot{\boldsymbol{q}} = \dot{\boldsymbol{H}}\dot{\boldsymbol{q}} - \frac{1}{2}(\frac{\partial}{\partial\boldsymbol{q}}(\dot{\boldsymbol{q}}^T\boldsymbol{H}\dot{\boldsymbol{q}}))^T. \tag{22}$$

Equation (21) could be further rewritten as

$$\begin{aligned}
&\dot{V}(1 + \frac{1}{2}\frac{\beta}{V}\boldsymbol{q}^2 + \frac{1}{4}\frac{\alpha}{V}\dot{\boldsymbol{q}}^T\boldsymbol{H}\boldsymbol{q}) \\
&= -\alpha(\frac{1}{2}\dot{\boldsymbol{q}}^T\boldsymbol{H}\dot{\boldsymbol{q}} + \frac{1}{2}\alpha\dot{\boldsymbol{q}}^T\boldsymbol{H}\boldsymbol{q} + \frac{1}{2}\beta\boldsymbol{q}^T\boldsymbol{q}) \\
&\quad + \frac{1}{4}\alpha(\dot{\boldsymbol{q}}^T(\frac{\partial}{\partial\boldsymbol{q}}\boldsymbol{H})\dot{\boldsymbol{q}})^T\boldsymbol{q}^T + \boldsymbol{S}(\dot{\boldsymbol{q}} + \frac{1}{2}\alpha\boldsymbol{q}).
\end{aligned} \tag{23}$$

In the following, each term on the right of the equal sign in Eq. (23) will be evaluated.

Specially, for the first term, by using Eqs. (13) and (14), we have

$$\begin{aligned}
&\alpha(\frac{1}{2}\dot{\boldsymbol{q}}^T\boldsymbol{H}\dot{\boldsymbol{q}} + \frac{1}{2}\alpha\dot{\boldsymbol{q}}^T\dot{\boldsymbol{H}}\boldsymbol{q} + \frac{1}{2}\beta\boldsymbol{q}^2) \\
&= \alpha V = \frac{\sqrt{3}U_0}{2\sqrt{2M}}V^{1/2}.
\end{aligned} \tag{24}$$

For the second term, by Cauchy inequality and inequality (3), we have

$$\begin{aligned}
&\frac{1}{4}\alpha(\dot{\boldsymbol{q}}^T(\frac{\partial}{\partial\boldsymbol{q}}\boldsymbol{H})\dot{\boldsymbol{q}})^T\boldsymbol{q}^T \\
&= \frac{1}{4}\alpha[(\dot{\boldsymbol{q}}^T(\frac{\partial}{\partial q_1}\dot{\boldsymbol{H}})\dot{\boldsymbol{q}}), (\dot{\boldsymbol{q}}^T(\frac{\partial}{\partial q_2}\boldsymbol{H})\dot{\boldsymbol{q}})]^T\boldsymbol{q}^T \\
&\le \frac{1}{4}\alpha\sqrt{2}D\dot{\boldsymbol{q}}^2\|\boldsymbol{q}\|.
\end{aligned} \tag{25}$$

By using Eq. (16) and inequality (2), we obtain

$$\boldsymbol{q}^2 \le \frac{1}{\beta}(\dot{\boldsymbol{q}}^T\boldsymbol{H}\dot{\boldsymbol{q}} + \beta\boldsymbol{q}^2) \le \frac{4}{\alpha^2 M}V, \tag{26}$$

$$\dot{\boldsymbol{q}}^2 \le \frac{1}{m}(\dot{\boldsymbol{q}}^T\boldsymbol{H}\dot{\boldsymbol{q}}) \le \frac{1}{m}(\dot{\boldsymbol{q}}^T\boldsymbol{H}\dot{\boldsymbol{q}} + \beta\boldsymbol{q}^2) \le \frac{4}{m}V. \tag{27}$$

Then, substituting inequalities (26) and (27) and into (25), we obtain

$$\frac{1}{4}\alpha(\dot{\boldsymbol{q}}^T(\frac{\partial}{\partial\boldsymbol{q}}\boldsymbol{H})\dot{\boldsymbol{q}})^T \le \frac{2\sqrt{2}D}{m\sqrt{M}}V^{3/2}. \tag{28}$$

For the third term, by Cauchy inequality and inequalities (2) and (5), we obtain

$$\begin{aligned}
&\|\boldsymbol{S}^T(\dot{\boldsymbol{q}} + \frac{1}{2}\alpha\boldsymbol{q})\| \le S_0\sqrt{\|\dot{\boldsymbol{q}} + \frac{1}{2}\alpha\boldsymbol{q}\|^2} \\
&= S_0\sqrt{\dot{\boldsymbol{q}}^2 + \frac{1}{4}\alpha^2\boldsymbol{q}^2 + \alpha\boldsymbol{q}^T\dot{\boldsymbol{q}}} \le S_0\sqrt{\frac{5}{4}(\dot{\boldsymbol{q}}^2 + \alpha^2\boldsymbol{q}^2)}, \\
&\le S_0\sqrt{\frac{5}{4}(\frac{1}{m}\dot{\boldsymbol{q}}^T\boldsymbol{H}\dot{\boldsymbol{q}} + \frac{\beta}{M}\boldsymbol{q}^2)}, \\
&\le S_0\sqrt{\frac{5}{4}\frac{1}{m}(\dot{\boldsymbol{q}}^T\boldsymbol{H}\dot{\boldsymbol{q}} + \beta\boldsymbol{q}^2)} \le S_0\sqrt{\frac{5}{m}V}.
\end{aligned} \tag{29}$$

Let us introduce a new notation

$$B = 1 + \frac{1}{2}\frac{\beta}{V}\boldsymbol{q}^2 + \frac{1}{4}\frac{\alpha}{V}\dot{\boldsymbol{q}}^T\boldsymbol{H}\boldsymbol{q}. \tag{30}$$

Finally, substituting Eq. (24), inequalities (28)-(30) into (23), we obtain

$$B\dot{V} \le -\frac{\sqrt{3}U_0}{2\sqrt{2M}}V^{1/2} + \frac{2\sqrt{2}D}{m\sqrt{M}}V^{3/2} + S_0\sqrt{\frac{5}{m}}V^{1/2} \tag{31}$$

Next, let us prove the positive-definiteness of $\boldsymbol{B}$ for any $(\boldsymbol{q}, \dot{\boldsymbol{q}})$.

Using Eqs. (14) and (30), we have

$$B = \frac{1}{V}(\frac{1}{2}\dot{\boldsymbol{q}}^T\boldsymbol{H}\dot{\boldsymbol{q}} + \beta\boldsymbol{q}^2 + \frac{3}{4}\alpha\dot{\boldsymbol{q}}^T\boldsymbol{H}\boldsymbol{q}). \tag{32}$$

By Eq. (15) we have

$$\alpha\dot{\boldsymbol{q}}^T\boldsymbol{H}\boldsymbol{q} \ge -\frac{1}{2}\dot{\boldsymbol{q}}^T\boldsymbol{H}\dot{\boldsymbol{q}} - \frac{1}{2}\beta\boldsymbol{q}^2. \tag{33}$$

Substituting inequality (33) into Eq. (32), we obtain

$$\begin{aligned}
B &\ge \frac{1}{V}(\frac{1}{2}\dot{\boldsymbol{q}}^T\boldsymbol{H}\dot{\boldsymbol{q}} + \beta\boldsymbol{q}^2 + \frac{3}{4}(-\frac{1}{2}\dot{\boldsymbol{q}}^T\boldsymbol{H}\dot{\boldsymbol{q}} - \frac{1}{2}\beta\boldsymbol{q}^2)) \\
&= \frac{1}{V}(\frac{1}{8}\dot{\boldsymbol{q}}^T\boldsymbol{H}\dot{\boldsymbol{q}} + \frac{5}{8}\beta\boldsymbol{q}^2) \ge 0.
\end{aligned} \tag{34}$$

It is obvious that for any $(\boldsymbol{q},\dot{\boldsymbol{q}}) \neq (0,0)$, B is positive. Then, the inequality (31) could be rewritten as,

$$\dot{V} \leq -\frac{1}{B}\left(\frac{\sqrt{3}U_0}{2\sqrt{2M}} - \frac{2\sqrt{2}D}{m\sqrt{M}}V - S_0\sqrt{\frac{5}{m}}\right)V^{1/2}. \tag{35}$$

Hence, if we set U_0 and S_0 satisfying following inequality, the global negative definiteness of $\dot{V}$ must be obtained.

$$U_0 > 2\sqrt{\frac{10M}{3m}}S_0 + \frac{8D}{\sqrt{3}m}V(\boldsymbol{q}_0,\dot{\boldsymbol{q}}_0), \tag{36}$$

where $(\boldsymbol{q}_0,\dot{\boldsymbol{q}}_0)$ is the initial state of the system.

At this point, we achieve the conclusion that the system's equilibrium state, $(\boldsymbol{q},\dot{\boldsymbol{q}}) = (0,0)$, is globally asymptotically stable.

Bounded property Analysis:

It has been mentioned that the proposed control has the property of bound in norm. Next, we will give the relative theoretical proof.

In particular, according to the control input $\boldsymbol{U}$ and Cauchy inequality, we could obtained

$$\begin{aligned}\boldsymbol{U}^2 &= (\boldsymbol{k}_d\dot{\boldsymbol{q}})^2 + (\boldsymbol{k}_p\boldsymbol{q})^2 + 2(\boldsymbol{k}_d\dot{\boldsymbol{q}})^T(\boldsymbol{k}_p\boldsymbol{q}) \\ &\leq \frac{4}{3}((\boldsymbol{k}_d\dot{\boldsymbol{q}})^2 + (\boldsymbol{k}_p\boldsymbol{q})^2 + (\boldsymbol{k}_d\dot{\boldsymbol{q}})^T(\boldsymbol{k}_p\boldsymbol{q})).\end{aligned} \tag{37}$$

Then, substituting the first equation of Eqs. (12) and (13) into Eq. (37), it has

$$\begin{aligned}\boldsymbol{U}^2 &\leq \frac{4}{3}\left(\frac{\beta}{M}(\boldsymbol{H}\dot{\boldsymbol{q}})^2 + \beta^2\boldsymbol{q}^2 + (\alpha\boldsymbol{H}\dot{\boldsymbol{q}})(\beta\boldsymbol{q})\right), \\ &\leq \frac{8}{3}\beta\left(\frac{1}{2}\dot{\boldsymbol{q}}^T\boldsymbol{H}\dot{\boldsymbol{q}} + \frac{1}{2}\beta\boldsymbol{q}^2 + \frac{1}{2}\alpha\dot{\boldsymbol{q}}^T\boldsymbol{H}\boldsymbol{q}\right).\end{aligned} \tag{38}$$

Finally, according to Eq. (14) and the second equation of Eqs. (13), we obtain

$$\boldsymbol{U}^2 \leq \frac{8}{3}\beta V = U_0^2. \tag{39}$$

The proof of the boundary property of the control input (6) is completed.

As mentioned above, the control input $\boldsymbol{U}$ is a function of the Lyapunov function V, but which is an implicit function. A practical problem will be faced is the solution of the V.

In particular, substituting Eqs. (13) into (14), it could been got

$$16V^2 = 8\dot{\boldsymbol{q}}^T\boldsymbol{H}\dot{\boldsymbol{q}}V + 3U_0^2\boldsymbol{q}^2 + \frac{2\sqrt{6}U_0^2}{\sqrt{M}}\dot{\boldsymbol{q}}^T\boldsymbol{H}\boldsymbol{q}V^{1/2}. \tag{40}$$

Then, introducing the following notations

$$\begin{aligned}&x = V^{1/2}, \quad \xi = 2\sqrt{2\dot{\boldsymbol{q}}^T\boldsymbol{H}\dot{\boldsymbol{q}}}, \\ &\eta = \frac{2\sqrt{6}U_0}{\sqrt{M}}\dot{\boldsymbol{q}}^T\boldsymbol{H}\boldsymbol{q}, \quad \gamma = \sqrt{3}U_0\|\boldsymbol{q}\|,\end{aligned} \tag{41}$$

and substitute Eqs. (41) into Eq. (40), we obtain the following equation.

$$16x^4 - \xi^2x^2 - \eta x - \gamma^2 = 0. \tag{42}$$

Moreover, there is a theorem [37]: if the coefficients satisfy the inequality,

$$\xi^2 + \gamma^2 > 0, \quad |\eta| \leq |\xi\gamma|. \tag{43}$$

Equation (42) must have a real root. The root must be positive and unique.

For our problem here, for any $(\boldsymbol{q},\dot{\boldsymbol{q}}) \neq (0,0)$, we have

$$\xi^2 + \gamma^2 = 8\dot{\boldsymbol{q}}^T\boldsymbol{H}\dot{\boldsymbol{q}} + 3U_0^2\boldsymbol{q}^2 > 0, \tag{44}$$

$$\eta^2 = 24\frac{U_0^2}{M}(\dot{\boldsymbol{q}}^T\boldsymbol{H}\boldsymbol{q})^2 \leq 24U_0^2(\dot{\boldsymbol{q}}^T\boldsymbol{H}\dot{\boldsymbol{q}})^2\boldsymbol{q}^2 = \xi^2\gamma^2. \tag{45}$$

Hence, in this paper, the value of V can be obtained by solving equation (42) using Newton iterative method. Then, the value of control gains $\boldsymbol{k}_p$, $\boldsymbol{k}_d$ and the control input $\boldsymbol{U}$ could be obtained in turn.

4 Experiments and results

In order to verify performance of the proposed control, a hardware experimental platform is designed, and several sets of experimental results are presented and analysed. Additionally, it has been found that the shake oscillation affects the autoloader the most in practice, so only the shake oscillation was considered in the experiment.

4.1 Hardware Platform

As shown in Fig. 4, our experimental platform is a scaled model of the above-mentioned autoloader. It mainly consists of three mechanical components: a lifting part, a revolving part and a mounted frame. Moreover, two servomotors are used to drive the lifting part and revolving part. Furthermore, both motors are equipped with digital encoders in the rears, which can provide a certain number of pulses per revolution and in turn the feedback signals of the motor shaft's angular position and velocity for the system control. Additionally, in order to reduce the speed of the motors and increase their output torques, two planetary-gear reducers are fitted between the mechanical devices and the relative servomotors. Moreover, above servomotors, encoders and reducers are all from MAXON company.

The control module of the experimental platform includes two digital positioning controllers (EPOS2 controllers provided by MAXON) and a Lenovo 32-bit personal computer. For achieving parallel control of the lifting part and the revolving part simultaneously, the master-slave communication technique is used in our experiments. Particularly, the

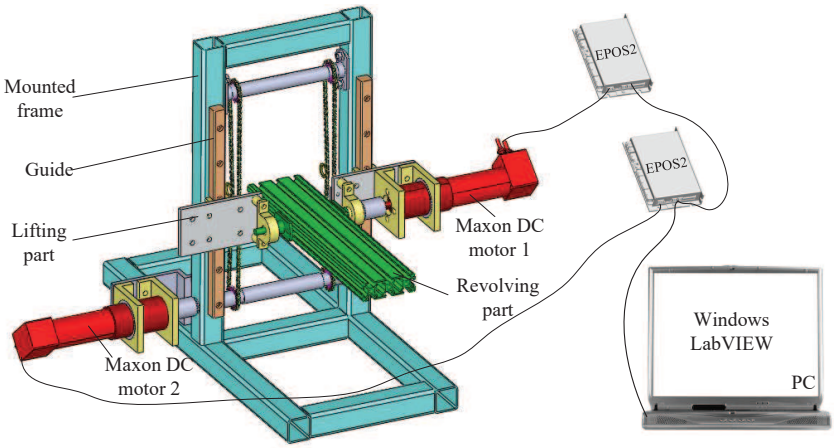

Fig. 4 Principle of the hardware platform

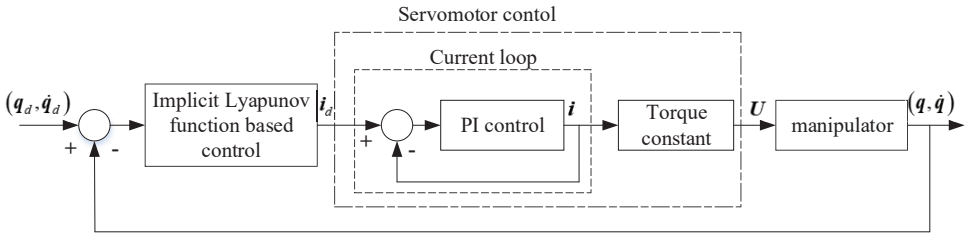

Fig. 5 Control loop of the experimental system

two EPOS2 controllers communicate as slaves, and the PC communicates as a master. Moreover, the CANopen communication protocol is used to transmit and receive data between the master (PC) and the slaves (EPOS2 controllers).

The EPOS2 controller has the typical three-loop-control (current-position-velocity) strategy embedded. However, in our experiments, only the built-in current-control-loop is adopted, while the position-velocity loops are replaced by a self-built loop based on the proposed control method. Moreover, the inner (current-control) loop adopts proportional-integral (PI) control. As shown in Fig. 5, it can be seen that the two control loops are connected by the torque constant of the servomotors. Additionally, our real-time control program was developed and successfully implemented in LabVIEW programming environments based on a Windows DLL file which contains some basic EPOS2 commands.

The overview of the experimental hardware system is presented in Fig. 6. As shown in the figure, the mechanical device is mounted on an electromagnetic vibration table (provided by ETS Solution Beijing Ltd), which can simulate the chassis vibration of the combat vehicle on the move.

Moreover, according to the control input's boundary property (6) and the linear relationship between the torque and current of the motor, we can obtain that the desired currents of the motors satisfies the condition.

$$\sqrt{c_{d1}^2 + (0.013 c_{d2})^2} \leq C \tag{46}$$

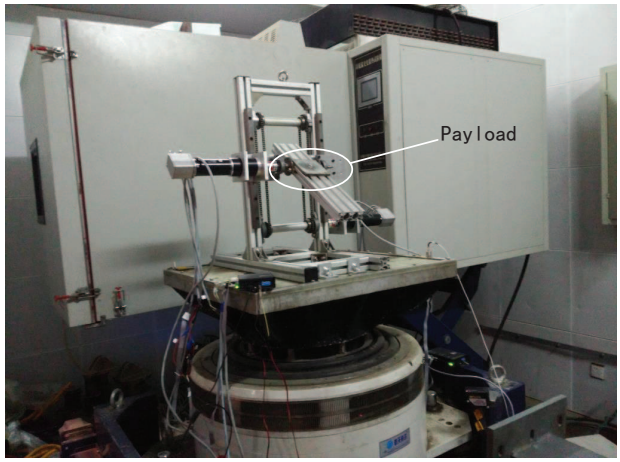

Fig. 6 Photograph of hardware platform

where c_{d1} and c_{d2} are desired currents for lifting motor and revolving motor respectively. Particularly, we finally obtain $C = 3600mA$ after some calculation.

Other system parameters are set as: $m_2 = 5kg$, $m_3 = 1kg$, $J = 0.01kg \cdot m^2$, $L_3 = 0.05m$, $m = 0.01$, $M = 8$, $U_0 = 800$, $S_0 = 200$, $D = 0.01$ and the gravitational acceleration equals to $9.8m/s^2$. Moreover, the original point is set as the terminal state of the stabilizing control, and the initial state is set as $(q_{10}, \dot{q}_{10}, q_{20}, \dot{q}_{20}) = (0.144, 0, -0.524, 0)$. In addition,

the PI gains of the current loop control is are respectively tuned as $k_{p1} = 352, k_{I1} = 92$ and $k_{p2} = 217, k_{I2} = 62$ for lifting part and revolving part, respectively.

4.2 Experiment results

Based on the above experimental platform, five cases of hardware experiments was implemented.

The Case 1 experiment is a contrast one, there is no base oscillations ($\boldsymbol{S} = 0$) nor payload uncertainty. The Case 2 experiment is to certify the control is robust to the real base oscillation. The base oscillation data is from our previous work, a simulation study of tracked vehicles maneuverability by ADAMS/ATV software. Moreover, due to current studies on OBMs control mostly used traditional sinusoid base oscillations, another contrast experiment was carried out as the Case 3 experiment. The amplitude and frequency of the sinusoid oscillation are $10mm$ and $36rad/s$, respectively.

In order to further prove the control's robustness against to payload uncertainty, two more cases of experiments were implemented. One is the case of considering the payload uncertainty only (Case 4) and the other for the case of both payload uncertainty and base oscillation are took into account (Case 5). For the case of payload uncertainty, an additional mass block is installed on the centroid of the revolving part, the mass of which is 0.4kg.

To illustrate the control's performance more clearly, results of these experiments are divided into two groups, as shown in Tab. 2.

Tab. 2 Experiment groups

Group NO.	Case NO.	Base Oscillation	Payload
Group I	Case 1	N/A	N/A
	Case 2	Real oscillation	N/A
	Case 3	Sinusoid oscillation	N/A
Group II	Case 1	N/A	N/A
	Case 4	N/A	0.4 kg
	Case 5	Real oscillation	0.4 kg

Group I: In this group, to illustrate the control's robustness against to the base oscillations, we firstly present the results of Case 1, Case 2 and Case 3 experiments.

The corresponding experimental results are presented in Fig. 7. Particularly, the black, blue and red curves stand for the case of no base oscillation, base oscillation from previ-

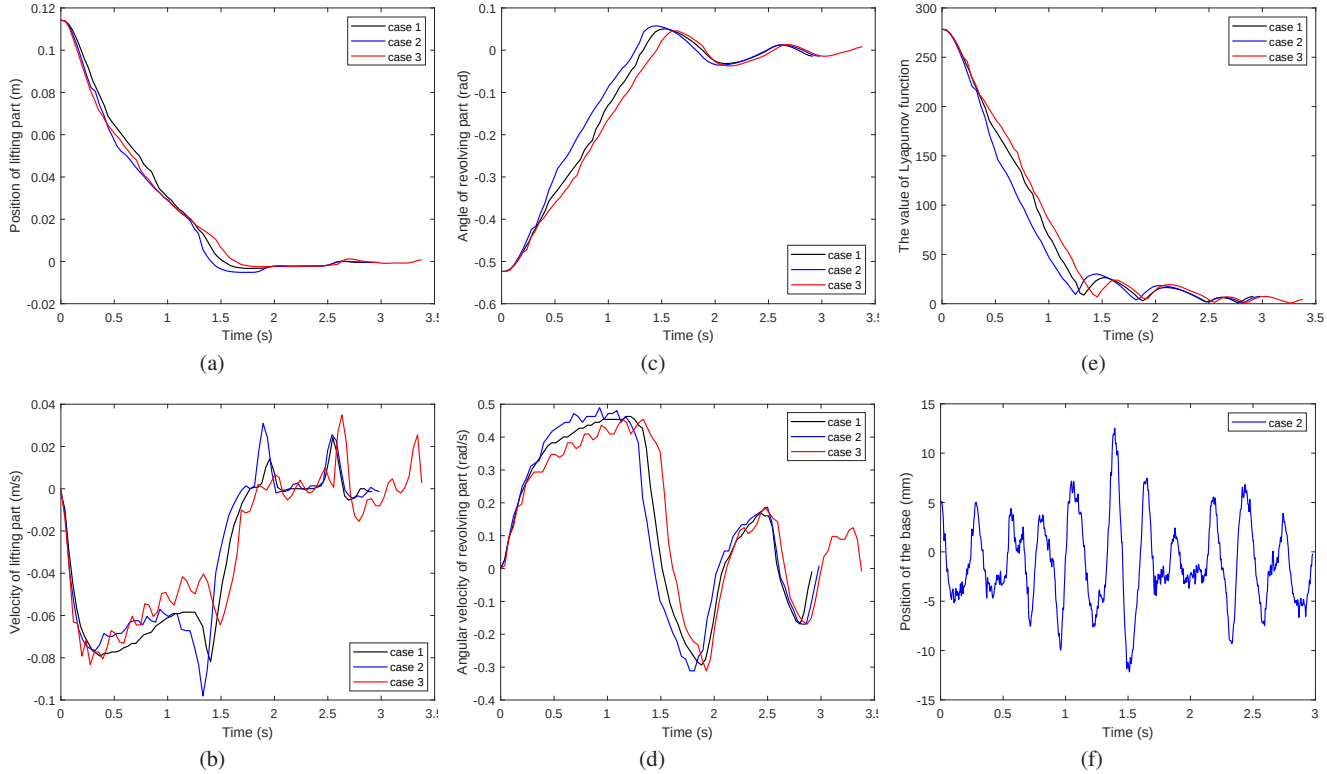

Fig. 7 Results of Group II. (a) Position of the lifting part. (b) Velocity of the lifting part. (c) Angle of the revolving part. (d) Angular velocity of the revolving part. (e)Lyapunov function. (f) Base oscillation.

ous simulation and sinusoidal base oscillation, respectively. It can been seen form Fig. 7a- Fig. 7d that, for all cases, the system converge towards the terminal state in a very short time. This proves that the proposed controller has good robustness to disturbances caused by base oscillations. However, we can also see that it takes more time for the case of base oscillations in comparison with no base oscillation, and case of sinusoidal base oscillation took the most time. In particular, the setting times are 2.915 seconds (without base oscillation), 3.01 seconds (base oscillation from previous simulation), 3.38 seconds (sinusoidal base oscillation), respectively. Moreover, it can be found that the response curves of angular velocity exhibit obvious oscillation characteristics especially for the case of sinusoidal base oscillation. Hence, it can been concluded that the frequency of the base oscillation will affect the system dynamic response. Fig. 7e is the responses the implicit Lyapunov function. Clearly, for both cases, the function approaches the terminal state non-monotonically. The reason is that the value of U_0 we chosen is much smaller than the requirement of sufficient condition (36). This results further present the implicit Lyapunov control's effectiveness. Additionally, Fig. 7f presents the base oscillation responses of case 2.

Group II: In this group, to further illustrate the control's robustness against to payload uncertainty, the results of Case 4 and Case 5 experiments are presented. Moreover, as a contrast case, the Case 1 experiment result is also presented here.

Corresponding results are shown in Fig. 8. By contrast, experimental results of case 1 (without neither oscillation nor payload uncertainty) are still presented here. Specifically, the black, green and brown solid lines in the figure correspond to the case of neither payload uncertainty nor base oscillation, only payload uncertainty, both payload uncertainty and base oscillation, respectively. As can be seen from Fig. 8a- Fig. 8d, the system takes 3.01 seconds and 3.311 seconds approaching to the terminal state for the two new cases, respectively. Obviously, the payload uncertainty, as did base oscillation, leads to a longer settling time of control compared with the case of neither base oscillation nor payload uncertainty. Moreover, it can see from Fig. 8e that the Lyapunov function curves also exhibit non-monotonically decreasing behavior, due to the sufficient condition (36) is not satisfied. Nevertheless, the control can steer the system approaching to terminal state. At this point, we obtain the conclusion that the proposed control has good robust performance against to not only base oscillation but also payload uncertainty. In addition, Fig. 8f is the position response of

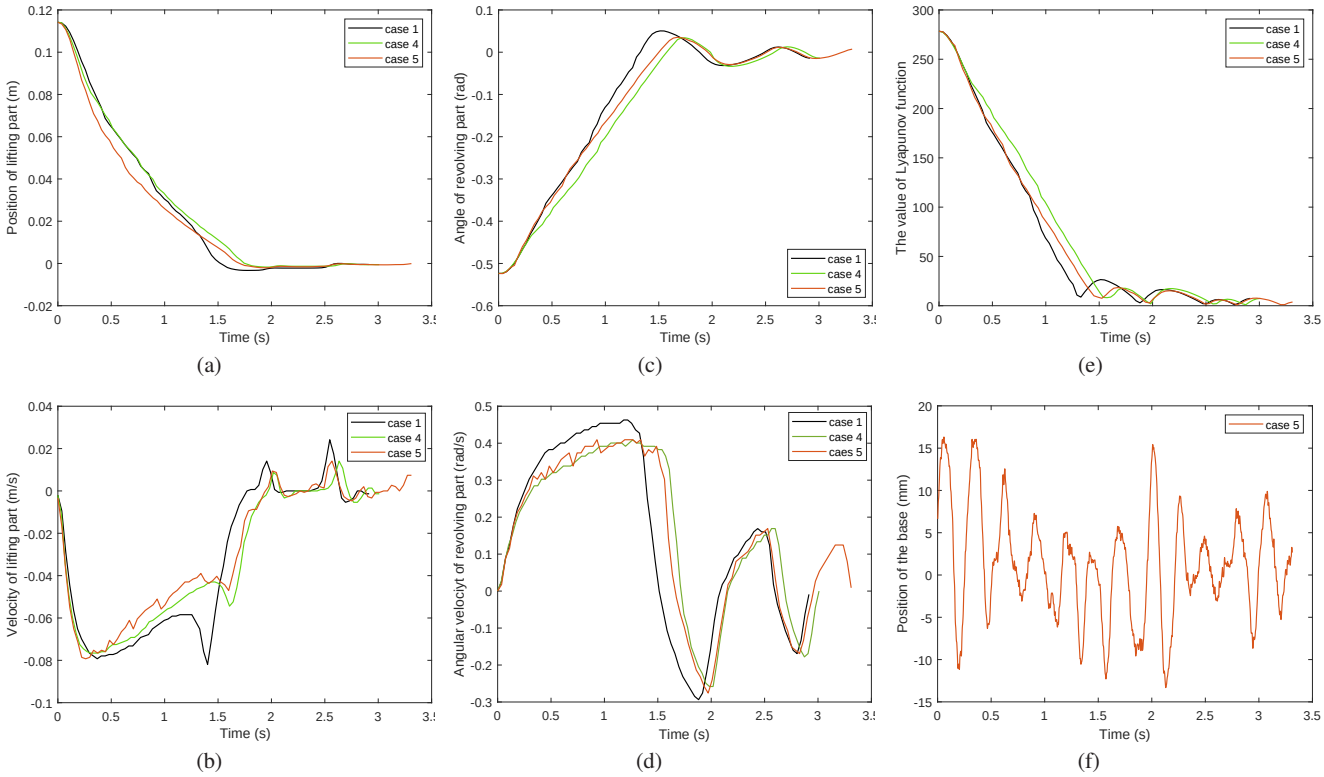

Fig. 8 Results of Group II. (a) Position of the lifting part. (b) Velocity of the lifting part. (c) Angle of the revolving part. (d) Angular velocity of the revolving part. (e)Lyapunov function. (f) Base oscillation.

the oscillatory base.

Furthermore, Fig. 9 presents the tracking responses of the current loops, in which the dashed-dot and solid lines present desired current and actual current, respectively. Moreover, the upper sub-figure presents lifting part's response. The bottom sub-figure are the results of revolving part. It can been seen from the figure that the actual currents achieved good tracking performance to the desired currents. This proves the effeteness of the current-loop's PI control. Moreover, we can also see that the desired currents, which were calculated based on control input of mechanical system, are always satisfying the condition (42). This proved the designed control's property as shown in inequality (6), and it can be conclude that the control is always bounded in norm.

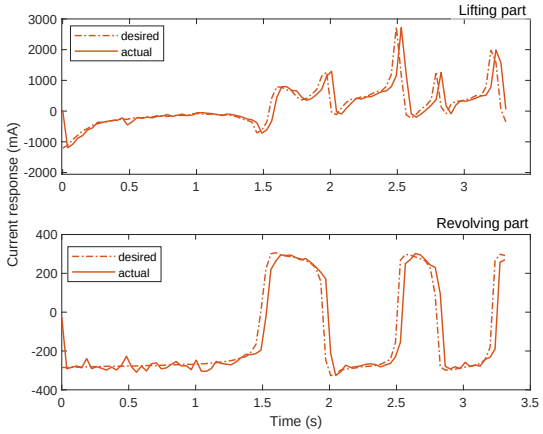

Fig. 9 Experiment results of the current responses of Case 5

5 Conclusion

In the presence of chassis oscillations and payload uncertainty, this paper have proposed a robust stabilizing control scheme for the MBT autoloaders. The proposed control method has several advantages and originality comparing with the existing researches. It has had the ability to deal with the uncertain chassis-oscillation-induced perturbations without the predictions or measurements of the chassis oscillations. It has also exhibited good robustness against payload uncertainty. Moreover, the proposed control has always been bounded in norm. Results of several hardware experiments has further proved that the proposed control has offered good performance in practice.

Acknowledgment

This work was supported by the National Natural Science Foundation of China (No. 51605344 and 51175266), the State Scholarship Fund from China Scholarship Council (No. 201908420154), and the grant from China Postdoctoral Science Foundation funded project (No. 2016M592398).

Declarations

Conflict of interest The authors have no conflicts of interest to declare that are relevant to the content of this article.

Data statement All the experimental data used in this paper are available from the corresponding author upon reasonable request.

References

1. Guo, Y., Hou, B.: Implicit Lyapunov function-based tracking control of a novel ammunition autoloader with base oscillation and payload uncertainty, *Nonlinear Dyn.*, 2017, **87**, (2), pp. 741-753.
2. Guo, Y., Xi, B., Huynh, V.T., *et al.*: Robust tracking control of MBT autoloaders with oscillatory chassis and compliant actuators, *Nonlinear Dyn.*, 2020, **99**, (3), 2185-2200.
3. Toda, M.: Robust motion control of oscillatory-base manipulators, (Springer, Switzerland, 2016)
4. Lin, J., Huang, Z.Z.: A hierarchical fuzzy approach to supervisory control of robot manipulators with oscillatory bases, *Mechatronics*, 2007, **17**, (10), pp. 589-600.
5. Yang, T.W., Xu, L.W., Han, J.D.: Dynamic compensation control of flexible macro-micro manipulator systems, *IEEE Trans. Control Syst. Technol.*, 2010, **18**, (1), pp. 143-151.
6. Mannani, A., Talebi, H.A.: A fuzzy Lyapunov-based control strategy for a macro-micro manipulator: experimental results, *IEEE Trans. Control Syst. Technol.*, 2007, **15**, (2), pp. 375-383.
7. Zong, L., Luo, J., Wang, M., *et al.*: Parameters concurrent learning and reactionless control in post-capture of unknown targets by space manipulators, *Nonlinear Dyn*, 2019, **96**, (1), pp. 443-447.
8. Roberto, L., Hrishik, M., Oumer, N.W., *et al.*: Tracking control for the grasping of a tumbling satellite with a free-floating robot, *IEEE Robot Autom. Lett.*, 2018, **3**, (4), pp. 3638-3645.
9. Simetti, E., Casalino, G.: Manipulation and transportation with cooperative underwater vehicle manipulator systems, *IEEE J. Ocean. Eng.*, 2017, **42**, (4), pp. 782-799.
10. Zhang, J., Li, W., Yu, J., *et al.*: Development of a virtual platform for telepresence control of an underwater manipulator mounted on a submersible vehicle, *IEEE Trans. Ind. Electron.*, 2017, **64**, (2), pp. 1716-1727.

11. Esfahania, H., Azimirada, V., Danesh, M.: A time delay controller included terminal sliding mode and fuzzy gain tuning for underwater vehicle-manipulator systems, *Ocean Eng.*, 2015, **107**, pp. 97-107.
12. Olguin-Diaz, E., Arechavaleta, G., Jarquin, G., *et al.*: A passivity-based model-free force-motion control of underwater vehicle manipulator systems, *IEEE Trans. Robot.*, 2013, **29**, (6), pp. 1469-1484.
13. Chen, H., Fang, Y., Sun, N., *et al.*: Optimal trajectory planning and tracking control method for overhead cranes, *IET Control Theory Appl.*, 2016, **10**, (6), pp. 692-699.
14. Sun, N., Fang, Y., Chen, H., *et al.*: Nonlinear stabilizing control for ship-mounted cranes with ship roll and heave movements: design, analysis, and experiments, *IEEE Trans. Syst. Man Cybern. Sys.*, 2018, **48**, (10), pp. 1781-1794.
15. Sun, N., Fang, Y., Chen, H., *et al.*: Nonlinear antiswing control of offshore cranes with unknown parameters and persistent ship-induced perturbations: theoretical design and hardware experiments, *IEEE Trans. Ind. Electron.*, 2018, **65**, (3), pp. 2629-2641.
16. Wongratanaphn, T., Cole, M.: Robust impedance control of a flexible structure mounted manipulator performing contact tasks, *IEEE Trans. Robot*, 2009, **25**, (2), pp. 445-451.
17. Rybus, T., Seweryn, K., Sasiadek, J.Z.: Control system for free-floating space manipulator based on nonlinear model predictive control(NMPC), *J. Intell. Robot. Syst.*, 2017, **85**, (3-4), pp. 491-507.
18. Xu, S., Wang, H., Zhang, D., *et al.*: Adaptive zero reaction motion control for free-floating space manipulators, *IEEE Trans. Aerosp. Electron. Syst.*, 2016, **52**, (3), pp. 1067-1076.
19. Nanos, K., Papadopoulos, E.: Avoiding dynamic singularities in cartesian motions of free-floating manipulators, *IEEE Trans. Aerosp. Electron. Syst.*, 2015, **51**, (3), pp. 2305-2318.
20. Wang, Y., Wang, S., Wei, Q., *et al.*: Development of an underwater manipulator and its free-floating autonomous operation, *IEEE/ASME Trans. Mechatron.*, 2016, **21**, (2), pp. 815-824.
21. Londhe, P.S., Santhakumar, M., Patre, B.M., *et al.*: Task space control of an autonomous underwater vehicle manipulator system by robust single-input fuzzy logic control scheme, *IEEE J. Ocean. Eng.*, 2017, **42**, (1), pp. 13-28.
22. Lynch, B., Ellery, A.: Effucuebt control of an AUV-manipulator system: an application for the exploration of europa, *IEEE J. Ocean. Eng.*, 2014, **39**, (3), pp. 552-570.
23. Leban, F.A., Diaz-Gonzalez, J., Parker, G.G., *et al.*: Inverse kinematic control of a dual crane system experiencing base motion, *IEEE Trans. Control Syst. Technol.*, 2015, **23**, (1), pp. 331-339.
24. Yang, Y., Wei, Y., Lou, J., *et al.*: Dynamic modeling and adaptive vibration suppression of a high-speed macro-micro manipulator, *J. Sound Vib.*, 2018, **442**, (1), pp. 318-342.
25. Wang H., Xie, Y.: Passivity based adaptive Jacobian tracking for free-floating space manipulators without using spacecraft acceleration, *Automatic.*, 2019, **45**, (2), pp. 1510-1517.
26. Tang, C., Wang, Y., Wang, S., *et al.*: Floating autonomous manipulation of the underwater biomimetic vehicle-manipulator system: methodology and verification, *IEEE Trans. Ind. Electron.*, 2018, **65**, (6), pp. 4861-4870.
27. Han, J., Chung. W.K.: Active use of restoring moments for motion control of an underwater vehicle-manipulator system, *IEEE J. Ocean. Eng.*, 2014, **9**, (1), pp. 100-109.
28. Wang, H., Guo, D., Chen, W., *et al.*: Eye-in-hand tracking control of a free-floating space manipulator, *IEEE Trans. Aerosp. Electron. Syst.*, 2017, **53**, (4), pp. 1855-1865.
29. Jiang, W., Wang, Z., Mourelatos, Z.P.: Application of nonequidistant fractional-order accumulation model on trajectory prediction of space manipulator, *IEEE/ASME Trans. Mechatron.*, 2016, **24**, (3), pp. 1420-1427.
30. Chu, Z., Cui, J., Sun, F.: Fuzzy adaptive disturbance-observer-based robust tracking control of electrically driven free-floating space manipulator, *IEEE Syst. J.*, 2014, **8**, (2), pp. 343-352.
31. Yurchenko D., Alevras, P.: Stability, control and reliability of a ship crane payload motion, *Prob. Eng. Mech.*, 2014, **38**, pp. 173-179.
32. Kuchler, S., Mahl, T., Jorg, N., *et al.*: Active control for an offshore crane using prediction of the vessel's motion, *IEEE/ASME Trans. Mechatron.*, 2011, **16**, (2), pp. 297-309.
33. Schaub, H.: Rate-based ship-mounted crane payload pendulation control system, *Control Eng. Pract.*, 2005, **16**, (2), pp. 132-145.
34. Toda, M.: An H_∞ control-based approach to robust control of mechanical systems with oscillatory bases, *IEEE Trans. Rob. Autom.*, 2004, **20**, (2), pp. 283-269.
35. Sato, M., Toda, M.: Robust motion control of an oscillatory-base manipulator in a global coordinate system, *IEEE Trans. Ind. Electron.*, 2015, **62**, (2), pp. 1163-1174.
36. Ananevskii, I.M.: Synthesis of continuous control of a mechanical system with an unknown inertia matrix, *J. Comput. Syst. Sci.*, 2006, **45**, (3), pp. 356-367.
37. Chernousko, F.L., Ananievskii, I.M., Reshmin, S.A.: Control of nonlinear dynamical system (Springer,

Berlin, 2008)
38. Spong, M.W., Hutchinson, S., Vidyasagar, M.: Robot modeling and control (John Wiley & AMP Sons Inc, New York, United, 2005)

Figures

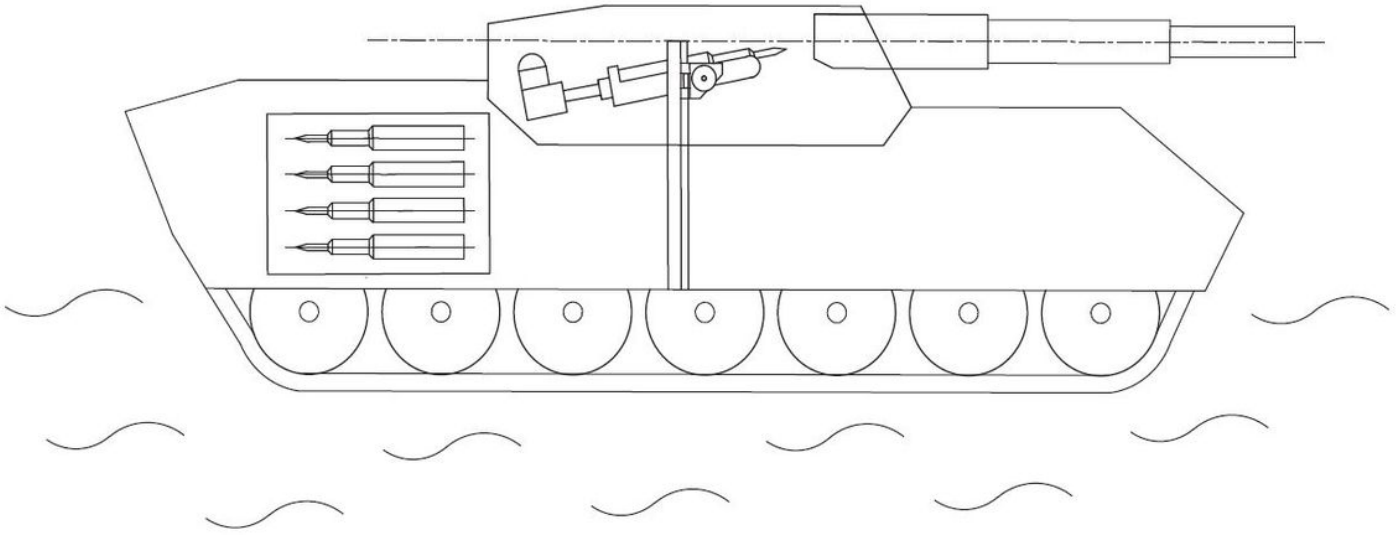

Figure 1

MBTs autoloader with oscillatory chassis

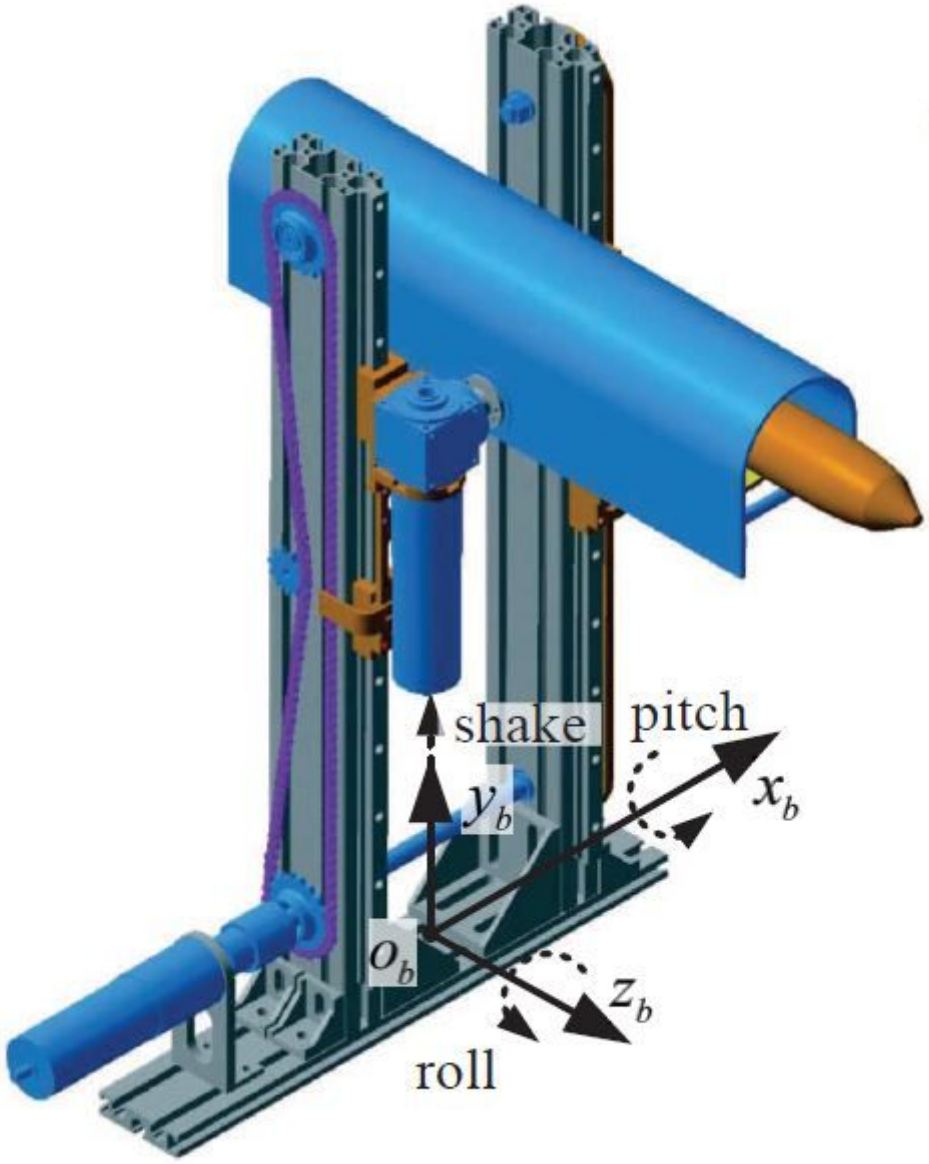

Figure 2

Virtual prototype of the autoloader

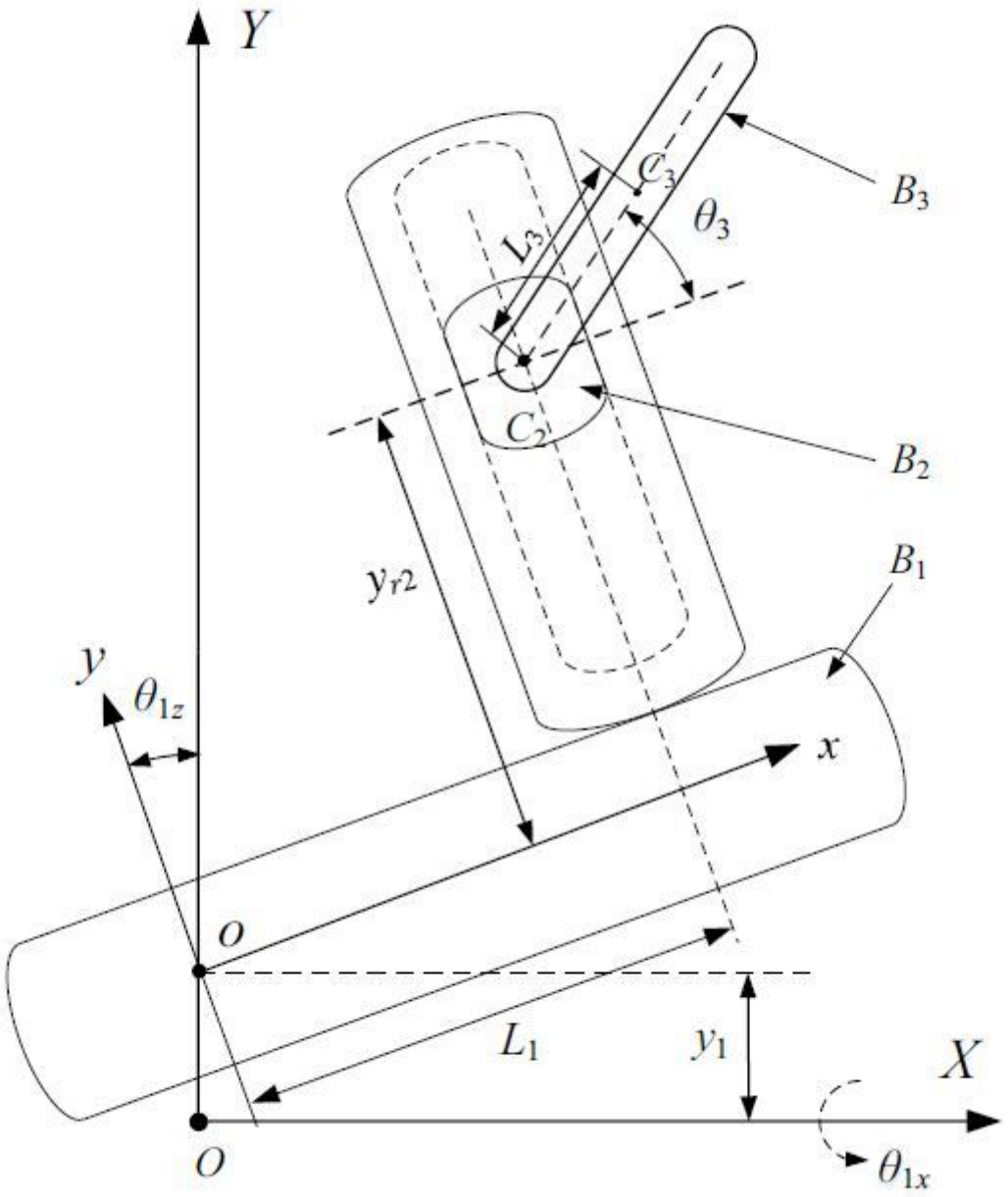

Figure 3

Simplified model of the autoloader with oscillatory base

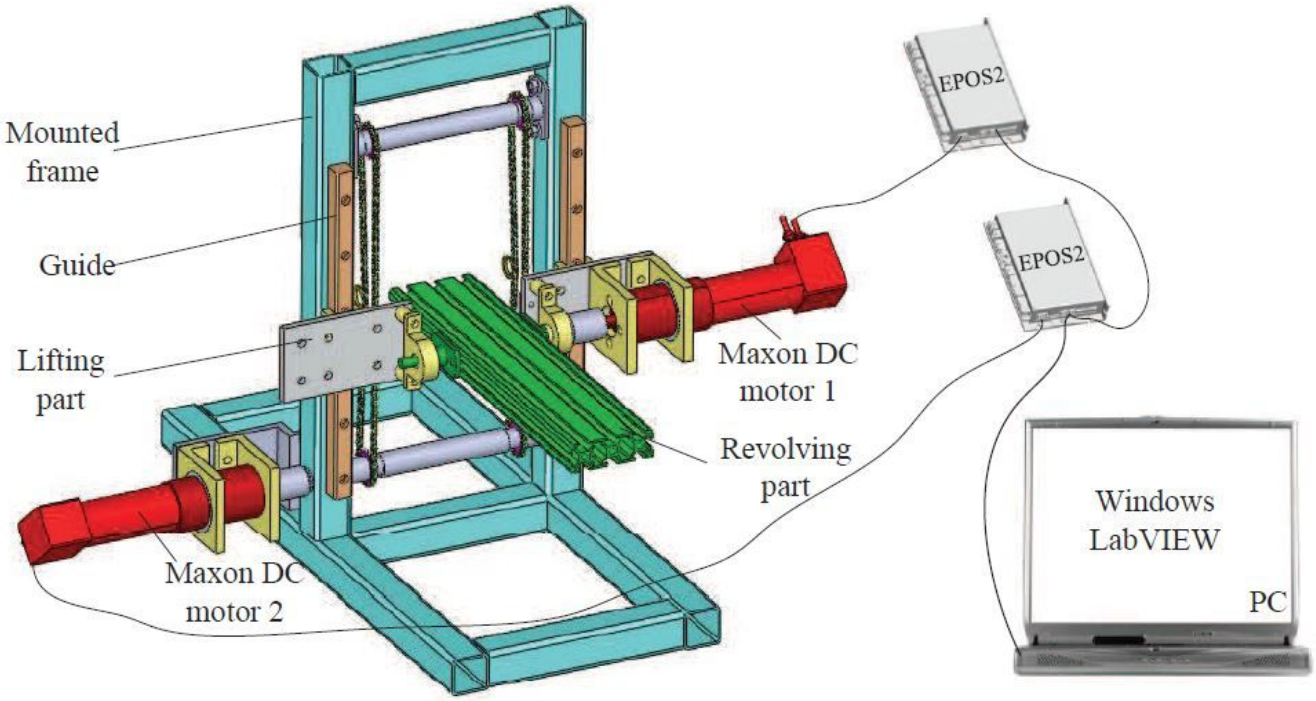

Figure 4

Principle of the hardware platform

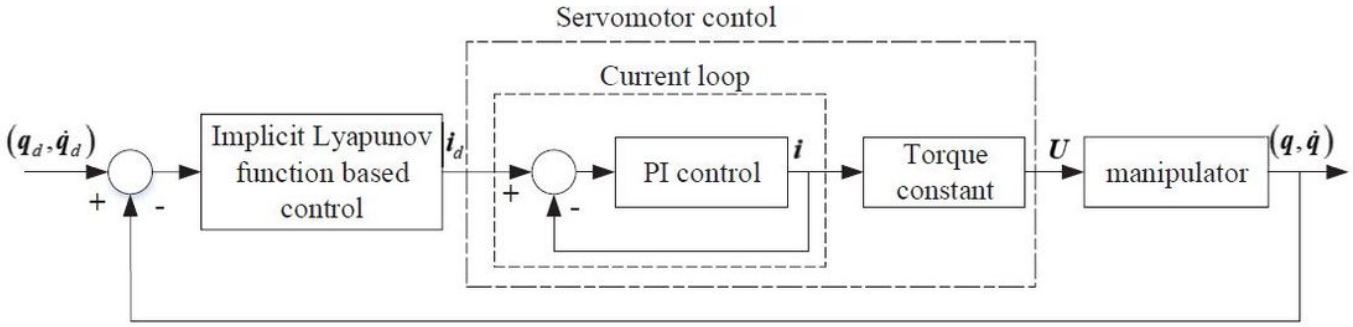

Figure 5

Control loop of the experimental system

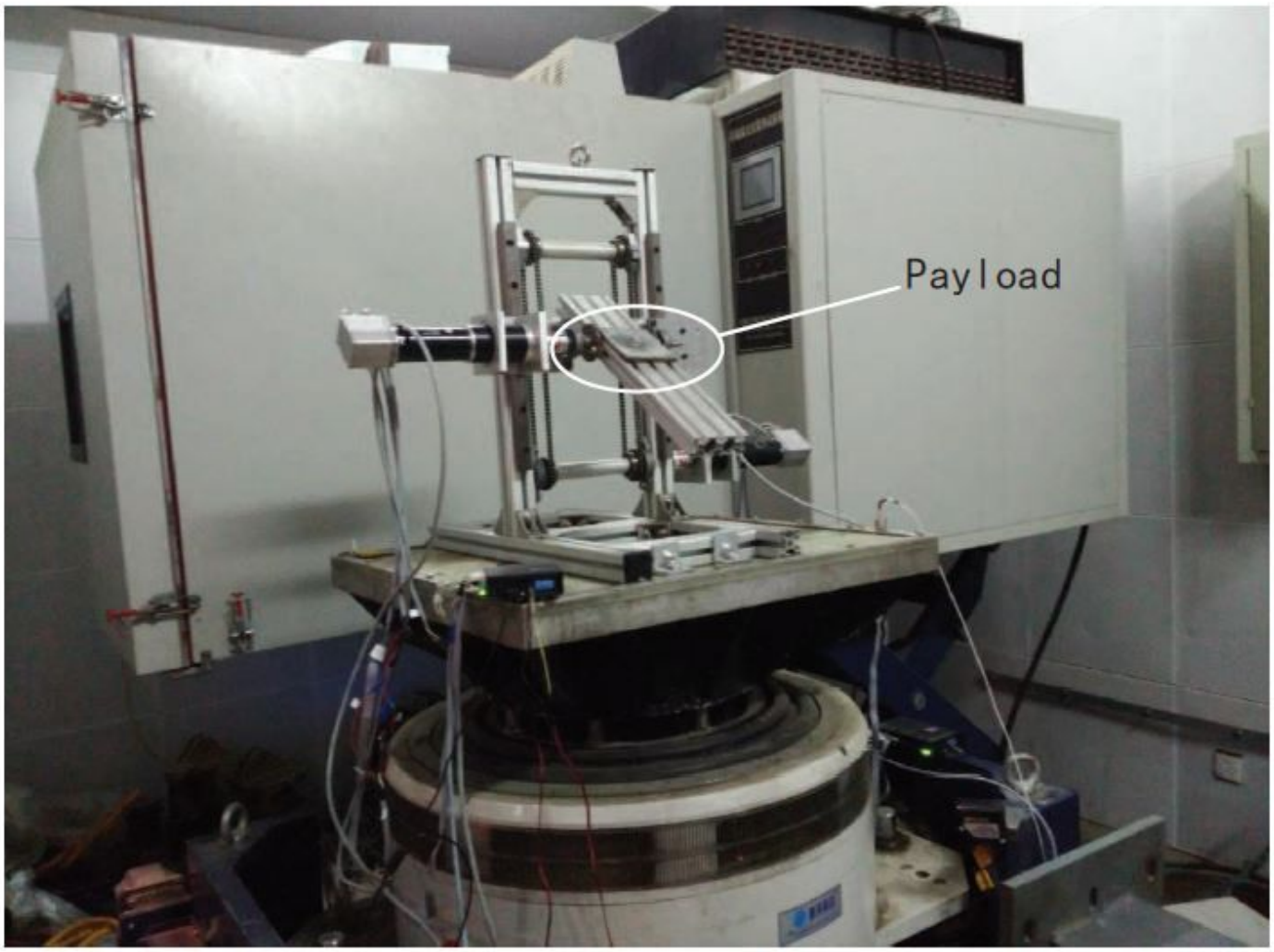

Figure 6

Photograph of hardware platform

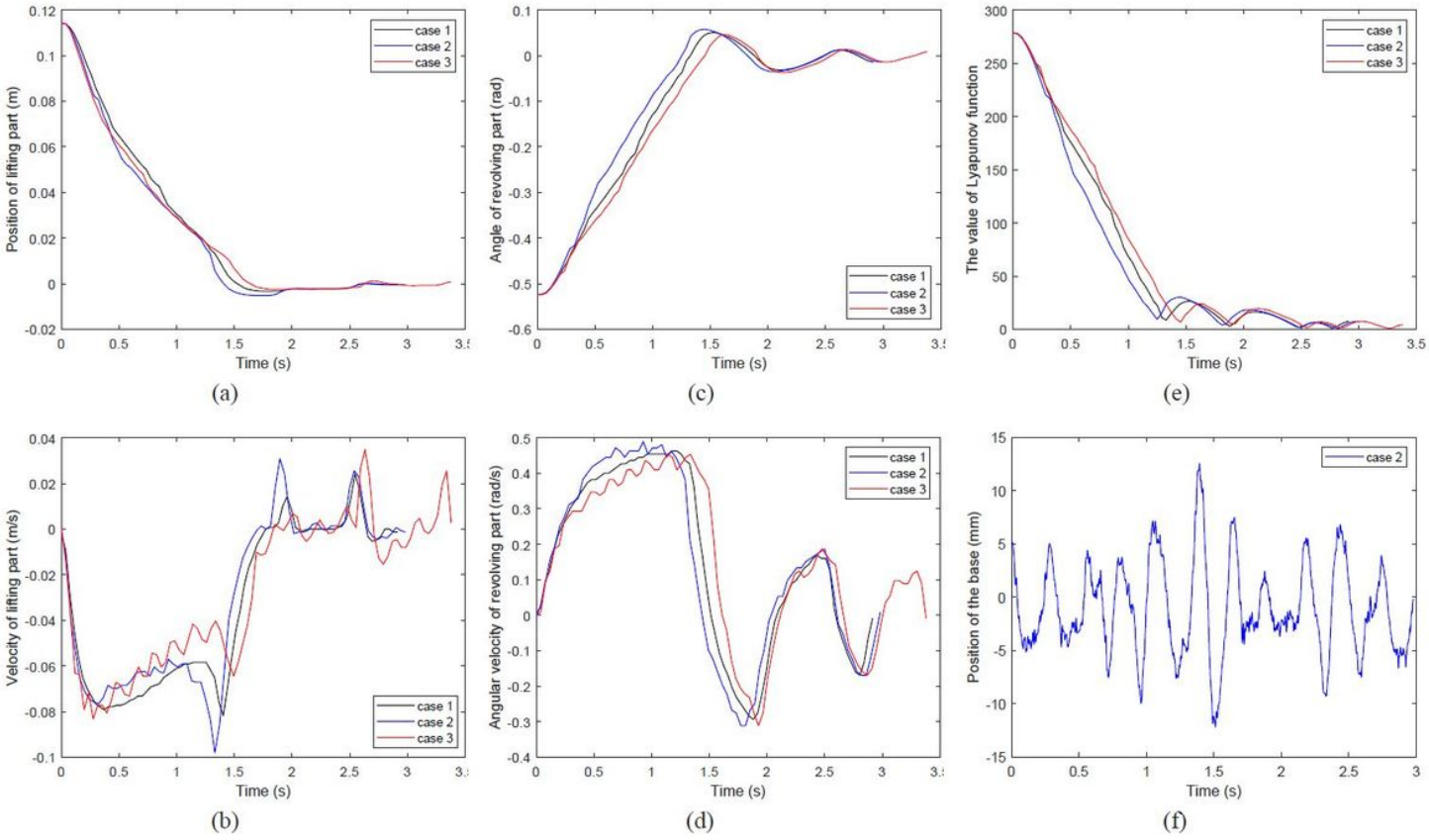

Figure 7

Results of Group II. (a) Position of the lifting part. (b) Velocity of the lifting part. (c) Angle of the revolving part. (d) Angular velocity of the revolving part. (e)Lyapunov function. (f) Base oscillation.

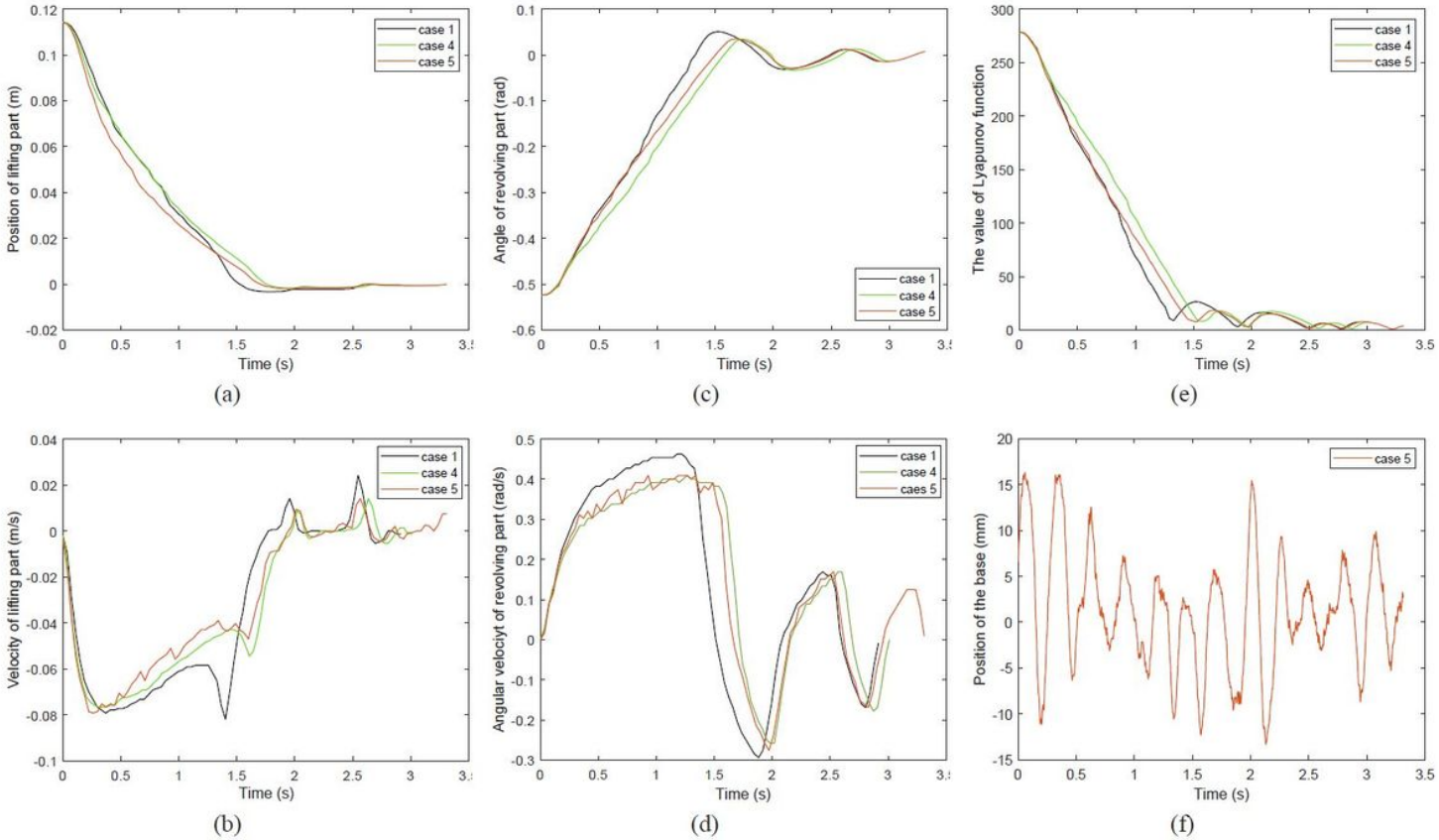

Figure 8

Results of Group II. (a) Position of the lifting part. (b) Velocity of the lifting part. (c) Angle of the revolving part. (d) Angular velocity of the revolving part. (e)Lyapunov function. (f) Base oscillation.

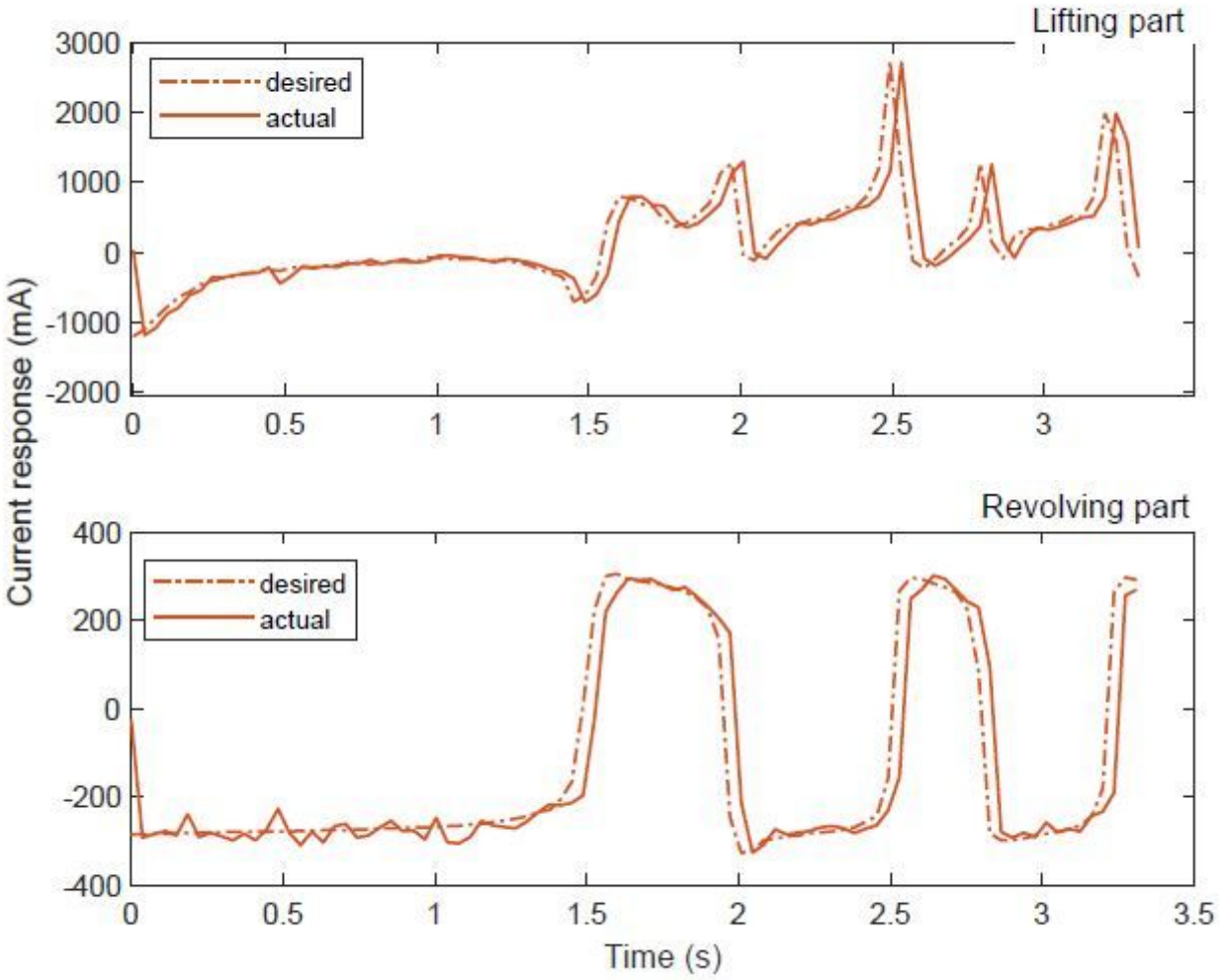

Figure 9

Experiment results of the current responses of Case 5

Supplementary Files

This is a list of supplementary files associated with this preprint. Click to download.

- Latexfileofthemanuscript.rar